

# Improving Texture Prediction by Increasing Mesh Resolution in Submodel: A Crystal Plasticity FE Study and Experiment Verification

Yu Liu <sup>1,2</sup>, Qi Zhang <sup>2</sup>, Qinqin Ge <sup>3</sup>, Xingxing Wang <sup>2</sup>  and Yifu Shen <sup>1,\*</sup> 

<sup>1</sup> College of Materials Science and Technology, NUAA, Nanjing 211106, China; liuyu\_me@ntu.edu.cn

<sup>2</sup> School of Mechanical Engineering, Nantong University, Nantong 226019, China; 2110110128@stmail.ntu.edu.cn (Q.Z.); wangxx@ntu.edu.cn (X.W.)

<sup>3</sup> Mechanical Maintenance Department, Nantong Cellulose Fibers Co., Ltd., Nantong 226007, China; 11317@ncfcinfo.com

\* Correspondence: yfshen\_nuaa@hotmail.com

**Abstract:** Crystal plasticity finite element simulations require tremendous computation time and, accordingly, coarse mesh is generally used. To improve the texture prediction, Submodelling was applied to feature grains in this study. A simulation of the Wholemodel (whole sample) was firstly carried out to obtain the global texture, and then a smaller region from the Wholemodel was selected, reconstructed and finely meshed in the Submodel. The movement on the selected region boundary, obtained from the Wholemodel, was used to deform the Submodel. The Submodel reproduced the predictions in the Wholemodel, and the texture prediction, especially at micro-scale, was greatly enhanced in the Submodel due to the fine mesh. This significant drop in the Submodel computation time marks an ~85% decrease compared to the Wholemodel.

**Keywords:** crystal plasticity FE; Submodel; mesh resolution; texture



**Citation:** Liu, Y.; Zhang, Q.; Ge, Q.; Wang, X.; Shen, Y. Improving Texture Prediction by Increasing Mesh Resolution in Submodel: A Crystal Plasticity FE Study and Experiment Verification. *Crystals* **2023**, *13*, 849. <https://doi.org/10.3390/cryst13050849>

Academic Editor: Pavel Lukáč

Received: 15 March 2023

Revised: 8 May 2023

Accepted: 10 May 2023

Published: 20 May 2023



**Copyright:** © 2023 by the authors. Licensee MDPI, Basel, Switzerland. This article is an open access article distributed under the terms and conditions of the Creative Commons Attribution (CC BY) license (<https://creativecommons.org/licenses/by/4.0/>).

## 1. Introduction

Texture modelling has become a powerful tool to predict metal deformation behaviours from macro- to micro-scale (e.g., [1,2]). Among these various crystal plasticity (CP) models, the so-called ‘full-field’ CP finite element (CPFE) model is supposed to be the best one for modelling the texture evolution [2–4]. The CPFE model introduces CP constitutive laws into the finite element (FE) package; the FE solves the boundary problems and the CP model is used to determine the plastic deformation at material points [5]. In each FE increment, the equilibrium in all elements is met with fundamental mechanical principles [2], which results in an obvious demerit: huge computation time. Increasing the mesh resolution is beneficial to improving the texture prediction [4,6–8], but reducing the element size results in a huge computation time. This explains why the mesh refinement ratios are very low in the literature, usually below 100 [5,6]. In this research, Submodelling was applied to a small region with fine mesh. The Submodel successfully reproduced the predictions in the Wholemodel, and the computation time was exceedingly reduced.

## 2. Materials and Experiments

High-purity aluminium alloy sheets were processed using rolling in this work. The material was fully annealed at 450 °C for 2 h, and sheet materials were cut into a dimension of 200 mm (length) × 40 mm (width) × 2 mm (thickness). The rolling at 50% reduction was performed on a rolling mill, consisting of 125 mm diameter rolls. After rolling, electron backscattered diffraction (EBSD) scans were performed to characterize the through-thickness textures on the rolling direction (RD)–normal direction (ND) plane. The EBSD samples were taken from the sheet centre, and the cross-section was mechanically

ground and then polished up to 1  $\mu\text{m}$  and finally electro-polished (16  $^{\circ}\text{C}$ , 25 V) in an A3 Struers electrolyte. EBSD scans were performed with a working distance of 15 mm and an accelerating voltage of 15 kV. HKL Channel-5 was used to postprocess the EBSD scanning.

### 3. Submodel Modelling

When employing FE modelling, there is a trade-off between computation time and mesh resolution, and thus the mesh refinement ratios are usually low. Submodelling is an alternative to assess a feature region, as this method is schematically shown in Figure 1. A coarse-mesh Wholemodel (whole sample) is firstly developed and then numerically solved. A critical part is selected and reconstructed in a fine-mesh Submodel. The displacement of nodes on the driven surface (in blue), which is extracted from the Wholemodel, acts as the boundary conditions for the Submodel, while the inner nodes (in green) are free to move according to the Submodel deformation.

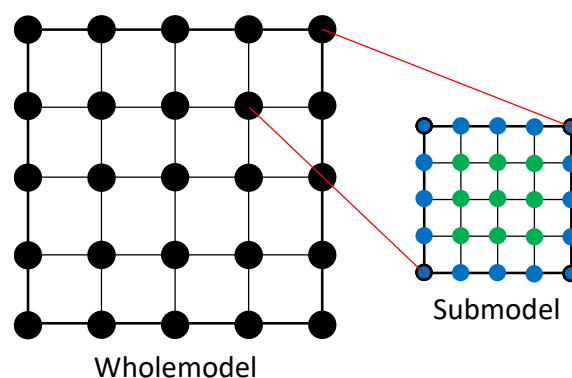
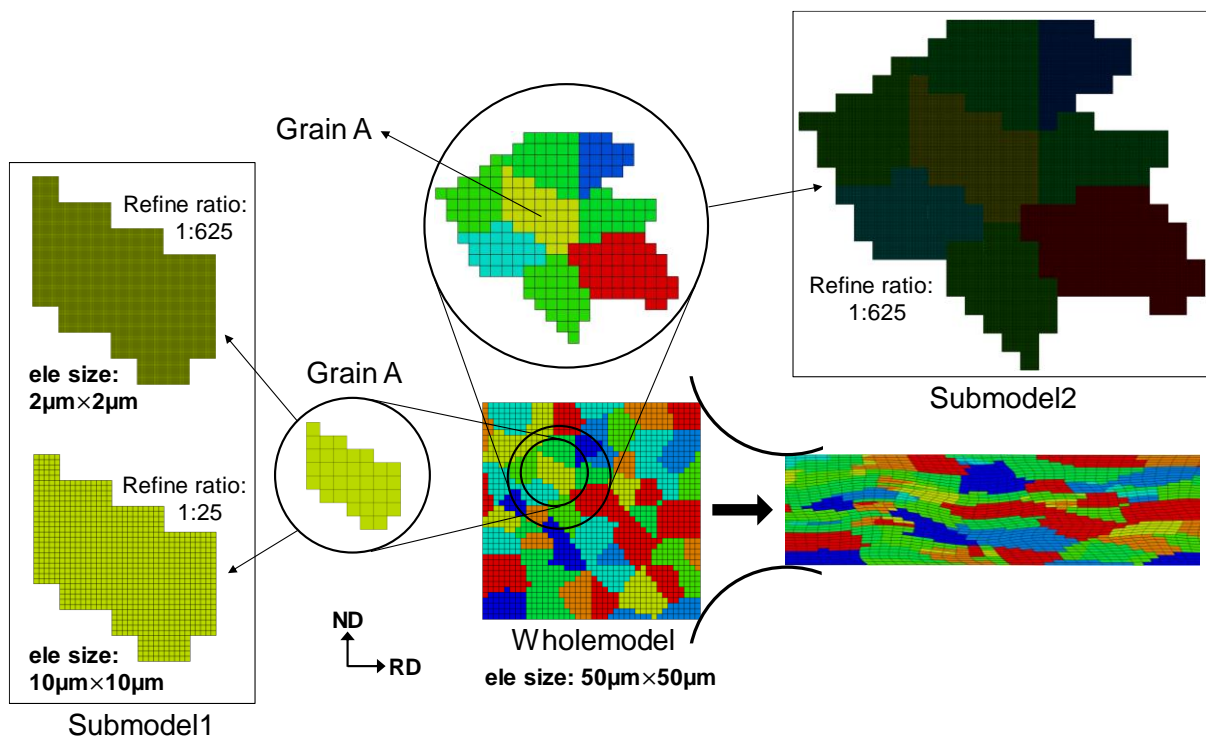


Figure 1. Submodel modelling method.

The simulation, following the experimental conditions and procedure, was carried out using the commercial FE package Abaqus/Standard ver.6.9. A two-dimensional FE model under plain-strain conditions was developed. The rolls (125 mm in diameter) were modelled as analytical rigid bodies. The element type is CPE4R, four-node elements with a reduced integration point. A polycrystal model with a coarse mesh (element size: 50  $\mu\text{m} \times 50 \mu\text{m}$ ), i.e., Wholemodel, was developed, as shown in Figure 2. After the Wholemodel, a feature region, Grain A in Figure 2, was reconstructed in the Submodel-1 and was then finely meshed with refinement ratios of 1:25 and 1:625. In the former and latter cases, one Wholemodel element was divided into 25 elements (element size: 10  $\mu\text{m} \times 10 \mu\text{m}$ ) and 625 elements (element size: 2  $\mu\text{m} \times 2 \mu\text{m}$ ), respectively. The element size of 2  $\mu\text{m} \times 2 \mu\text{m}$  in the Submodel-1 is comparably large as the step size used in EBSD scans. In the Submodel-2 (Figure 2), not only Grain A but also its neighbouring grains were included. Grain A in the Submodel-2 was driven by the neighbouring grains, which are supposed to apply relatively ‘soft’ boundary conditions on Grain A. When Submodelling, the initial grain orientations in both the Wholemodel and Submodel were kept the same.

The well-recognized kinematical scheme developed by Asaro [8] and the widely adopted Bassani–Wu hardening model [9,10] were used in this study. The material parameters were identified by matching the predictions to the experimental results compression [11]. Textures in different processes have been successfully captured by this CPFE model [3,12,13], which proves the reliability and capability of this CPFE model. The crystal plasticity constitutive law, hardening model and material parameters, as well as the CPFE implement, have been given in Ref. [3].



**Figure 2.** Mesh resolution of selected grains in Submodel and Wholemodel.

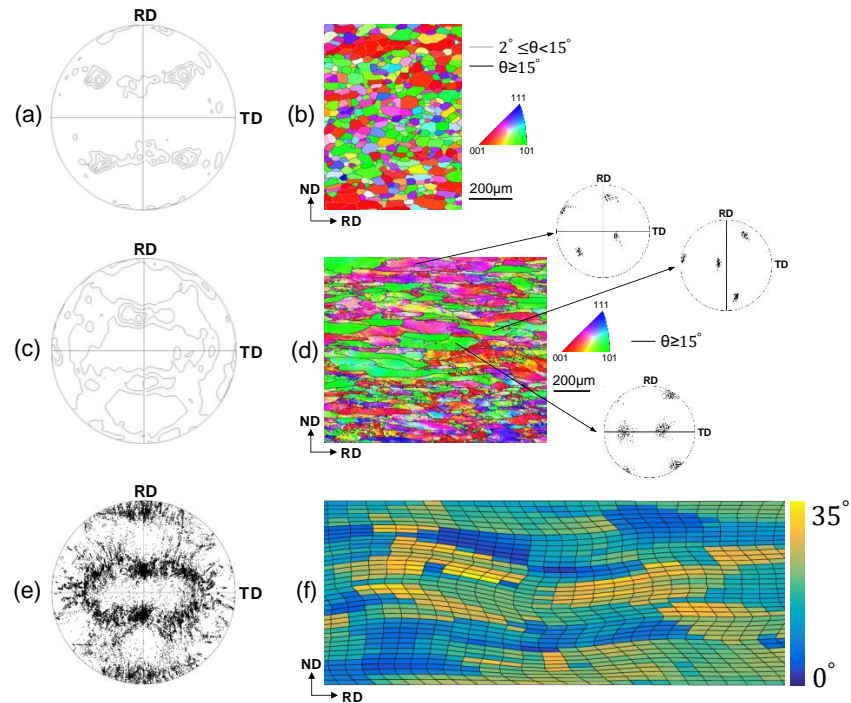
#### 4. Results

Figure 3a,b show a (1 1 1) pole figure and EBSD map of the starting material, respectively. The initial texture is a recrystallized texture, i.e., [5]  $\langle 0\ 0\ 1 \rangle$  Cube dominated (Figure 3a), and only a small number of low-angle grain boundaries (LAGBs) ( $2^\circ \leq \theta < 15^\circ$ ) in grains can be seen (Figure 3b). After rolling, the global texture evolved into a rolling texture (Figure 3c), typically consisting of  $\{1\ 1\ 2\}\langle 1\ 1\ 1 \rangle$ ,  $\{1\ 2\ 3\}\langle 6\ 3\ 4 \rangle$  and  $\{1\ 1\ 0\}\langle 1\ 1\ 2 \rangle$ . The high-angle grain boundaries (HAGBs) in Figure 3d are believed to be from the original ones but did not evolve during rolling, and the subgrain and LAGBs formed within the initially annealed grains. The pole figures of three representative grains are shown on the right of Figure 3d, from which it can be seen that an in-grain subdivision occurred and initially uniform in-grain orientations became scattered.

The predicted global texture from the Wholemodel (Figure 3e) reproduces the experimental observation in Figure 3c. After rolling, texture gradients developed in the Wholemodel (Figure 3f), which means an in-grain subdivision also occurred. However, compared to the step size in Figure 3d, the mesh resolution in the Wholemodel (Figure 3f) was exceedingly low. From Figure 3, it can be concluded that an acceptable global texture can be captured by the coarse-mesh Wholemodel.

The texture evolution of Grain A in the Wholemodel is shown in Figure 4a, and only a few elements were used to describe the in-grain texture; thus, the texture gradient is very high. As for the Submodel-1, a similar texture of Grain A was reproduced with the refinement ratio of 1:25 (Figure 4b), where the intensities of major texture components were strengthened and subtle components were also captured. The texture prediction was further improved by increasing the refinement ratio to 1:625 (Figure 4c), and macroscopic shear bands (marked by black arrows) and microscopic shear bands (red arrows) were also predicted. The predictions in the Submodel-2 1:625 (Figure 4d) are similar to those in Figure 4c in terms of shear bands and strong and weak texture components, although the grain shape is slightly different, since Grain A in the Submodel-2 was driven by the neighbouring grains, but not directly by its deformation history in the Wholemodel. The crystal rotation angles in the four models (shown in Figure 4) are similarly distributed in Figure 5. Although the fraction of relatively large rotation angles decreases slightly as the

mesh resolution increases, the distributions of all four models are generally consistent. This agrees with the slightly lowered average rotation angles of Grain A in the four models (Figure 4).



**Figure 3.** (1 1 1) pole figures of the global texture (a) before rolling, (c) after rolling and (e) in the Wholemodel. IPF EBSD maps (b) before rolling and (d) after rolling, and (f) distribution of crystal rotation angles in the Wholemodel.

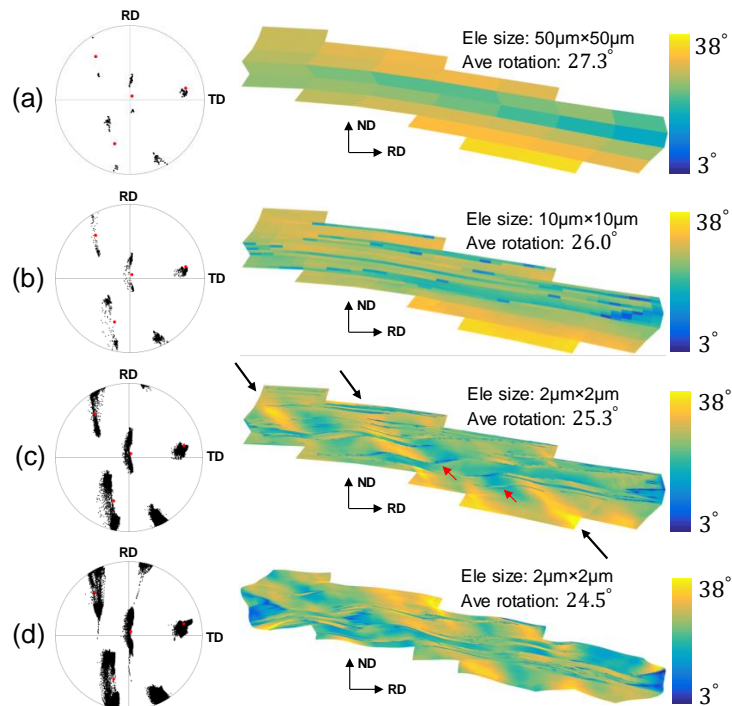


**Figure 4.** (1 1 1) pole figures and distribution of crystal rotation angles of Grain A in the (a) Wholemodel, (b) Submodel-1 1:25, (c) Submodel-1 1:625 and (d) Submodel-2 1:625. The initial orientations are shown in red, and final orientations in black. Black arrows indicate grain-scale shear bands, while micro-scale shear bands are marked by red arrows.

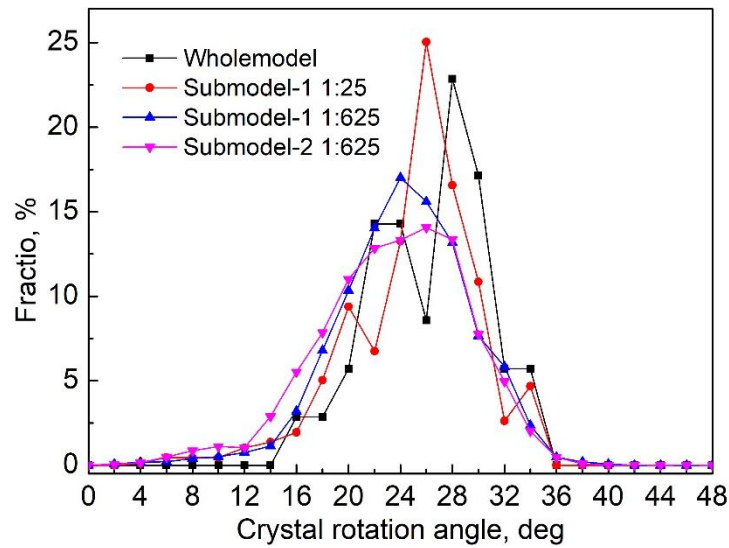


Figure 5. Distribution of crystal rotation angles in Grain A.

Figure 6 shows the CPU time at different refinement ratios. It can be seen that the computation time of the Wholemodel was reduced by about ~85% in the Submodel when the element number in them is the same. This is because complicated boundary conditions and interactions were considered when analysing the Wholemodel, and they cost expensive computation sources, while the boundary conditions for the Submodel are greatly simplified and thus the computation time is reduced. As for the Submodel with different mesh refinement ratios, it can be seen that the CPU time is almost linearly related to the element number. The CPU time increases ~17 times when the mesh refinement ratio is 625. When using the Submodel method, the computation time became affordable, especially for a relatively small region.

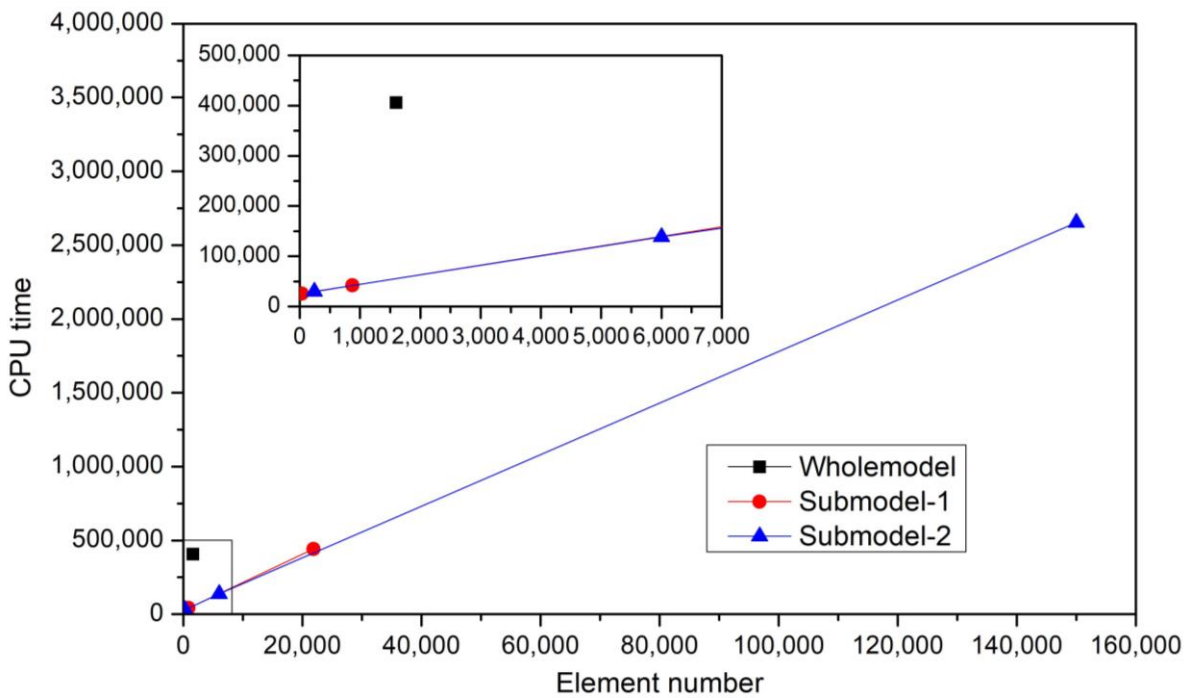


Figure 6. Relation between element number and CPU time in seconds.

### 5. Discussion

No homogenization is theoretically assumed in the CPFE model, but intra-element subdivision is not accessible (saying element type is CPE4R). Though the element size in

the Wholemodel was obviously larger than the EBSD step sizes, acceptable global textures have been predicted by the coarse mesh. In contrast, the texture prediction was greatly enhanced by reducing the element size in the Submodel in terms of major and minor texture components, as well as macro- and micro-scale shear bands. Increasing the mesh resolution means more elements are used to describe the textural gradients, so the subtle textures can be reasonably captured. Meanwhile, the material flow was enhanced, and this is why in-grain shear bands (Figure 4c,d) were predicted. Inherent length scale is not assumed in the current CPFE model [5,6] and there is no assumed homogenization, which implies that similar textures to those in the Wholemodel [5] can be reproduced in the Submodel. The boundary conditions of the Submodel were slightly altered (Figure 4d), but the alteration is negligible, as can be seen from the comparison of grain shapes and averaged rotation angles between the four models (Figures 4 and 5). Moreover, compared to external loading, the initial orientations of grains played a dominant role in the in-grain texture development [12]. With the affordable computation time, the refinement ratio reached a high number due to the reduced size of the sample in the Submodel. The maximum mesh refinement ratio is 625 in this study, but it is only 16 [5] and 30 [6] when fine meshes were applied to the whole sample. As an alternative, Submodelling is capable of reproducing predictions at an exceedingly reduced computation time. This study proves that Submodelling can be applied to feature regions in various FE simulations.

## 6. Conclusions

1. The global texture produced by the coarse-mesh Wholemodel agrees well with the experimental observations.
2. Submodelling was adopted to access the texture in a grain with highly refined mesh. The Submodel successfully reproduced the predictions in the Wholemodel, and more experimentally observed phenomena such as subtle texture components and shear bands were revealed in the Submodel.
3. The computation time for the Submodel was reduced by ~85% compared with the Wholemodel, because the complicated boundary conditions and interactions in the Wholemodel, which need much computation sources, were not considered in the Submodel.
4. Compared to the Wholemodel, the computation time of the Submodel was greatly saved due to the reduced region, and thus high-mesh resolution can be used in the Submodel. This study proves that Submodelling can be applied to feature regions in various FE simulations.

**Author Contributions:** Conceptualization, Y.L.; Data curation, Q.Z.; Formal analysis, Q.G. and Y.L.; Investigation, X.W.; Methodology, Y.L. and Y.S.; Project administration, Y.S.; Resources, Y.S.; Software, Y.L.; Supervision, Y.S.; Validation, Q.Z.; Visualization, Q.G.; Writing—original draft, Y.L.; Writing—review & editing, Y.L. All authors have read and agreed to the published version of the manuscript.

**Funding:** This research was funded by Natural Science Horizontal Research Project of Nantong University (grant number: 22ZH643) and A Project Funded by the Priority Academic Program Development of Jiangsu Higher Education Institutions (PAPD).

**Data Availability Statement:** Not applicable.

**Acknowledgments:** The authors would like to express their gratitude for the Natural Science Horizontal Research Project of Nantong University (grant number: 22ZH643) and A Project Funded by the Priority Academic Program Development of Jiangsu Higher Education Institutions (PAPD).

**Conflicts of Interest:** The authors declare no conflict of interest.

## References

1. Zhang, K.; Holmedal, B.; Hopperstad, O.S.; Dumoulin, S.; Gawad, J.; Van Bael, A.; Van Houtte, P. Multi-level modelling of mechanical anisotropy of commercial pure aluminium plate: Crystal plasticity models, advanced yield functions and parameter identification. *Int. J. Plast.* **2015**, *66*, 3–30. [[CrossRef](#)]
2. Van Houtte, P.; Li, S.; Seefeldt, M.; Delannay, L. Deformation texture prediction: From the Taylor model to the advanced Lamel model. *Int. J. Plast.* **2005**, *21*, 589–624. [[CrossRef](#)]

3. Wang, H.; Cheng, L.; Kiet, T.; Yu, L. A crystal plasticity FE study of macro- and micro-subdivision in aluminium single crystals {001}<110> multi-pass rolled to a high reduction. *J. Mater. Sci. Technol.* **2021**, *76*, 231–246.
4. Zhao, Z.; Kuchnicki, S.; Radovitzky, R.; Cuitiño, A. Influence of in-grain mesh resolution on the prediction of deformation textures in fcc polycrystals by crystal plasticity FEM. *Acta Mater.* **2007**, *55*, 2361–2373. [[CrossRef](#)]
5. Buchheit, T.E.; Wellman, G.W.; Battaile, C.C. Investigating the limits of polycrystal plasticity modelling. *Int. J. Plast.* **2005**, *21*, 221–249. [[CrossRef](#)]
6. Harewood, F.J.; McHugh, P.E. Investigation of finite element mesh independence in rate dependent materials. *Comput. Mater. Sci.* **2006**, *37*, 442–453. [[CrossRef](#)]
7. Inoue, T.; Tsuji, N. Quantification of strain in accumulative roll-bonding under unlubricated condition by finite element analysis. *Comput. Mater. Sci.* **2009**, *46*, 261–266. [[CrossRef](#)]
8. Asaro, R.J. Crystal Plasticity. *J. Appl. Mech. Trans. ASME* **1983**, *50*, 921–934. [[CrossRef](#)]
9. Wu, T.-Y.; Bassani, J.L.; Laird, C. Latent Hardening in Single Crystals I. *Theory Exp. Proc. R. Soc. A Math. Phys. Eng. Sci.* **1991**, *435*, 20.
10. Bassani, J.L.; Wu, T.-Y. Latent Hardening in Single Crystals II. *Anal. Charact. Predict. Proc. R. Soc. A Math. Phys. Eng. Sci.* **1991**, *435*, 21.
11. Wang, H.; Cheng, L.; Kiet, T. A Combined Experiment and Crystal Plasticity FEM Study of Microstructure and Texture in Aluminium Processed by Reverse and Unidirectional Accumulative Roll-Bonding. *Crystals* **2019**, *9*, 119. [[CrossRef](#)]
12. Wei, P.; Lu, C.; Tieu, K.; Su, L.; Deng, G.; Huang, W. A study on the texture evolution mechanism of nickel single crystal deformed by high pressure torsion. *Mater. Sci. Eng. A* **2017**, *684*, 239–248. [[CrossRef](#)]
13. Raabe, D.; Zhao, Z.; Mao, W. On the dependence of in-grain subdivision and deformation texture of aluminum on grain interaction. *Acta Mater.* **2002**, *50*, 4379–4394. [[CrossRef](#)]

**Disclaimer/Publisher’s Note:** The statements, opinions and data contained in all publications are solely those of the individual author(s) and contributor(s) and not of MDPI and/or the editor(s). MDPI and/or the editor(s) disclaim responsibility for any injury to people or property resulting from any ideas, methods, instructions or products referred to in the content.